GLOBAL BIOGEOCHEMICAL CYCLES, VOL. 27, 1013–1022, doi:10.1002/gbc.20093, 2013

Hysteresis conditions the vertical position of deep chlorophyll maximum in the temperate ocean

Gabriel Navarro [1] and Javier Ruiz [1]

Received 1 May 2012; revised 30 July 2013; accepted 27 September 2013; published 8 October 2013.

[1] Deep chlorophyll maxima (DCMs) are widespread features of oceans. In temperate regions, DCMs are commonly associated with isopycnal surfaces that frequently move over a wide vertical range. This general association between DCMs and isopycnals remains unexplained by present theories, and we show here that it emerges from the seasonal history of the water column. Analysis of the formation of more than 9000 seasonal DCMs throughout the world's oceans consistently locates the vertical position of spring/summer DCMs in temperate seas at the density of the previous winter mixed layer, independently of this density value and future depth. These results indicate that DCM formation cannot be understood without hysteresis by solely considering the instantaneous response of phytoplankton to vertical gradients in physical and chemical fields. Present theories for DCM formation cannot explain why spring and summer DCMs are systematically found at a density equal to that of the previous mixed layer where a bloom has occurred. Rather than reacting to instantaneous physical forcing, the results indicate that DCMs operate as self-preserving biological structures that are associated with particular isopycnals because of their capacity to modify the physicochemical environment. Combined with remote sensors to measure salinity and temperature in the surface ocean, this new understanding of DCM dynamics has the potential to improve the quantification of three-dimensional primary production via satellites. This significant enhancement of the representation of oceanic biological processes can also allow increasingly realistic predictions of future biogeochemical scenarios in a warming ocean.

Citation: Navarro, G., and J. Ruiz (2013), Hysteresis conditions the vertical position of deep chlorophyll maximum in the temperate ocean, *Global Biogeochem. Cycles*, *27*, 1013–1022, doi:10.1002/gbc.20093.

1. Introduction

[2] Maximum chlorophyll concentrations are commonly observed deep below the surface of stratified oceans [*Lonhgurst and Harrinson*, 1989; *Cullen*, 1982]. These deep chlorophyll maxima (DCM) are widespread features of oceans and account for a high proportion of their total chlorophyll content [*Takahashi and Hori*, 1984]. These DCMs are connected to phytoplankton biomass and are manifested as regions of high fluorescence in vertical profiles of water properties where oceans seasonally stratify [*Lonhgurst and Harrinson*, 1989]. Owing to their ubiquity and global significance for the biological functioning of pelagic ecosystems, various mechanisms have been proposed to explain their origin and maintenance.

[3] Hypotheses for their occurrence have explored the settling of phytoplankton [*Riley et al*., 1949] and its variation with depth [*Steele and Yentsh*, 1960] or light intensity [*Bienfang et al*., 1983], motility of flagellated phytoplankton, pycnoclines [*Jerlov*, 1959], and nutriclines [*Takahashi and Hori*, 1984] as the causes of seasonal DCMs. Other explanations set DCMs at the bottom of the euphotic zone [*Kirk*, 1983] or where a physiological increase of chlorophyll per cell occurs [*Cullen*, 1982], in connection with differential grazing pressure [*Lorenzen*, 1967] or alternatively emerging from a combination of the factors above [*Beckmann and Hense*, 2007; *Jamart et al*., 1977; *Lonhgurst and Harrinson*, 1989]. Numerical models have established the role of intraspecific competition for light and nutrients, caused by the upward and downward fluxes of nutrients and light, respectively, in determining DCMs [*Klausmeier and Litchman*, 2001]. This model has been included in subsequent simulation exercises [*Mellard et al*., 2011; *Ryabov et al*., 2010; *Yoshiyama and Nakajima*, 2002].

[4] Classical textbooks in biological oceanography [*Mann and Lazier*, 1991] explain DCMs in connection with vertical gradients in turbulence. Recently, modeling has demonstrated that the combination of these mechanisms can result in chaotic-like DCM dynamics [*Huisman et al*., 2006]. Table S1 (in the supporting information) provides a historical compilation of the different mechanisms proposed to explain DCMs location as well as the ocean regions where all of the hypothesis were proposed. The high diversity of hypotheses reflects the important role played by DCMs in biological

Additional supporting information may be found in the online version of this article.

[1]Department of Ecology and Coastal Management, Instituto de Ciencias Marinas de Andalucía, ICMAN-CSIC, Cadiz, Spain.

Corresponding author: G. Navarro, Instituto de Ciencias Marinas de Andalucía (ICMAN-CSIC), Campus Universitario Rio San Pedro, Avda. Republica Saharaui, 2, 11510 Puerto Real (Cádiz), Spain. (gabriel.navarro@icman.csic.es)

0886-6236/13/10.1002/gbc.20093

Table 1. CTD Profiles Data Sources[a]

CTD Profiles With Fluorescence and/or Chlorophyll Acronym	Source	No. of Profiles	Webpage
AMT	Atlantic Meridional Transect	414	http://www.amt-uk.org/
BATS	Bermuda Atlantic Time-series Study	1726	http://bats.bios.edu/
CalCOFI	California Cooperative Oceanic Fisheries Investigations	1067	http://www.calcofi.org/
CARIACO	Carbon Retention In A Colored Ocean Project	93	http://ocb.whoi.edu/jg/dir/OCB/CARIACO/
EDDIES	Eddies Dynamics, Mixing, Export, and Species composition	230	http://ocb.whoi.edu/jg/dir/OCB/EDDIES/
GLOBEC-NEP	Global Ocean Ecosystem Dynamics—North East Pacific	726	http://globec.whoi.edu/jg/dir/globec/nep/
US-GLOBEC Georges Bank	Global Ocean Ecosystem Dynamics—Georges Bank	3	http://globec.whoi.edu/jg/dir/globec/gb/
Gulf of Cádiz	P_3A_2, SESAME, GOLFO	224	http://www.sesame-ip.eu/
HOT	Hawaii Ocean Time-series	95	http://hahana.soest.hawaii.edu/hot/hot_jgofs.html
JAMSTEC	Japan Agency for Marine-Earth Science and Technology	563	http://www.godac.jamstec.go.jp/cruisedata/e/
US JGOFS NBP	U.S. JGOFS Southern NBP98	3	http://usjgofs.whoi.edu/jg/dir/jgofs/southern/nbp98_2/
NODC	National Oceanographic Data Center	2904	http://www.nodc.noaa.gov/
SEADA-TANET	Pan-European infrastructure for Ocean and Marine Data Management	692	http://www.seadatanet.org/
SOFeX	Southern Ocean Iron Experiment	29	http://ocb.whoi.edu/jg/dir/OCB/SOFeX/
TAO	Tropical Atmosphere Ocean project	182	http://www.pmel.noaa.gov/tao/
VERTIGO	Vertical Transport In the Global Ocean	176	http://ocb.whoi.edu/jg/dir/OCB/VERTIGO/
BBOP	Bermuda Bio-Optics Project		http://www.icess.ucsb.edu/bbop/Home.html

[a]JGOFS, joint global ocean flux study; SESAME, southern european seas: assessing and modelling ecosystem changes; GOLFO, Gulf of Cadiz Project.

oceanography and, on the other hand, highlights the large degree of postulation made about a phenomenon whose nature is not yet fully understood.

[5] One widespread feature of DCMs is their strong association with isopycnals rather than with depths [*Fasham et al.*, 1985; *Navarro et al.*, 2006]. When combined in a single plot, fluorescence profiles from an oceanic region frequently appear as scattered if plotted against depth. However, they collapse into similar curves when represented against potential density anomaly (σ_θ), and DCMs are constrained within a narrow range of σ_θ values. This is a broad pattern common to the temperate areas of the Atlantic and Pacific oceans as well as the Mediterranean Sea (Table S2 compiles examples of DCMs constrained at a specific σ_θ for different ocean regions). Despite the persistence of this extensive feature, much more effort has been devoted to understanding the mechanisms of DCM formation than to explaining why DCMs fit to a certain σ_θ. There is no apparent reason why the biological mechanisms proposed to originate DCMs, e.g., differential predation or photo acclimation, should be specifically activated at a certain σ_θ. Although competition for nutrients and light are known to determine the DCM [*Klausmeier and Litchman*, 2001], it is not evident why this competition always happen at a certain σ_θ. In particular, this association is more intriguing if we consider the wide range of depths in which this σ_θ may occur in the region and the strong physical and chemical gradients present in the water column.

[6] This manuscript postulates that the connection between DCMs and σ_θ can only be explained by considering the seasonal history of the water column in temperate waters. We propose that, rather than passively reacting to instant external forcing, DCMs modify the physical and chemical environment in such a way that they become self-preserving biological structures. Once DCMs originate at a certain σ_θ, the DCM controls the vertical distribution of nutrients and light through the competition mechanism identified by *Klausmeier and Litchman* [2001] to such an extent that they persist at that σ_θ. Our results, which are based on the analysis of the formation of more than 9000 seasonal DCMs throughout the world's ocean, suggest that this hysteresis effect is a common phenomenon in temperate oceans, and thereby, it cannot be ignored when understanding the formation and dynamics of DCMs in these regions.

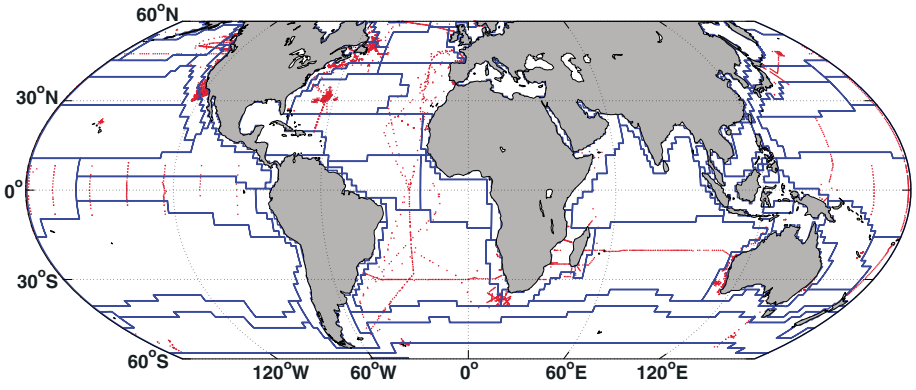

Figure 1. Spatial distribution (red dots) of all CTD profiles analyzed (Table 1). Background blue lines represent the Longhurst provinces [*Longhurst*, 1998].

Table 2. Acronyms Information

Acronym	Source	Units	Explanation
MLD_{GODAS}	GODAS model	m	Mixed layer depth (MLD) for each station and node
MLD^{MAX}_{GODAS}	GODAS model	m	Maximum value of the mixed layer depth
$\sigma_{\theta\ ML-GODAS}$	GODAS model	kg m^{-3}	Average density anomaly in the mixed layer for each station and node
$\sigma^{CHL}_{\theta ML-GODAS}$	GODAS model	kg m^{-3}	Average density anomaly in the mixed layer when the surface chlorophyll *a* derived from satellite data is at its maximum for each station and node
$\sigma_{\theta DCM}$	CTD profiles	kg m^{-3}	Density anomaly associated with the DCM for each CTD profile
$S^{CHL}_{ML-GODAS}$	GODAS model		Average salinity in the mixed layer when the surface chlorophyll *a* derived from satellite data is at its maximum for each station and node
S_{DCM}	CTD profiles		Salinity associated with the DCM for each CTD profile
CHL_{SAT}	Satellite GlobColour	mg m^{-3}	Weekly surface chlorophyll *a*
CHL_{max}	Satellite GlobColour	mg m^{-3}	Maximum concentration of the weekly surface chlorophyll *a*
CHL(*z*)	Scaled CTD profile	mg m^{-3}	Biomass profile derived from fluorescence profiles after scaling by satellite chlorophyll *a*
$CHL_{Gaussian}$	Equation (1) fitted to CHL(*z*)	mg m^{-3}	Biomass profile shifted to a Gaussian distribution function

2. Material and Methods

[7] In order to evaluate the effect of hysteresis on DCM formation, more than 9000 conductivity-temperature-depth (CTD) casts in the open ocean (>200 m depth) available from oceanographic databases (including fluorescence) have been used (Table 1 and Figure 1). In addition, satellite information has been employed to derive surface chlorophyll *a* and global model outputs to simulate mixed layer dynamics at the ocean.

3. Mixed Layer Information

[8] Monthly potential temperature, salinity, and mixed layer depth (MLD_{GODAS}, see Table 2 for acronym information) were determined from the ocean data assimilation model

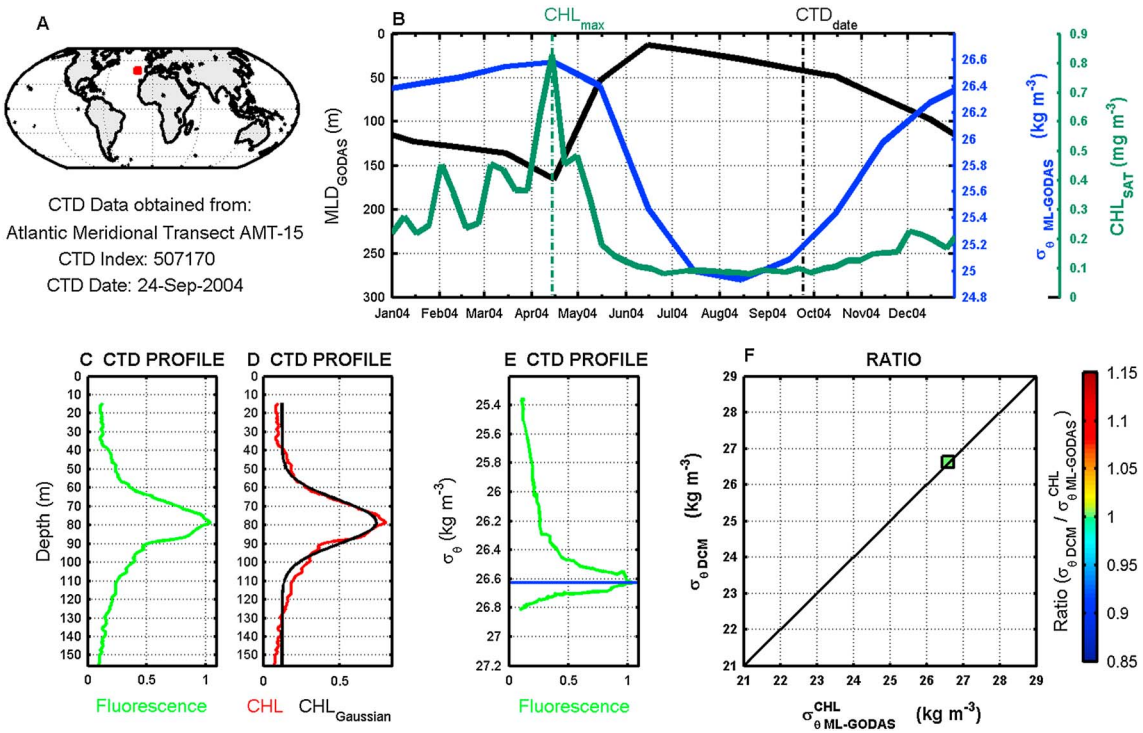

Figure 2. (a) Location of the CTD profile analyzed. (b) Time evolution of monthly mixed layer depth (MLD_{GODAS}, black line), average density anomaly values in the MLD_{GODAS} ($\sigma_{\theta\ ML-GODAS}$, blue line) and weekly satellite chlorophyll *a* (CHL_{SAT}, green line) for the CTD location. Vertical black and green dashed lines represent the dates of the CTD profile (CTD_{date}) and the surface chlorophyll *a* maximum (CHL_{max}), respectively. (c) Vertical profile of fluorescence in rfu (relative fluorescence units). (d) Vertical profile of chlorophyll concentration (red line, in mg m^{-3}) derived from fluorescence and vertical profile of chlorophyll concentration (black line, in mg m^{-3}) fitted to a shifted Gaussian distribution function. (e) Fluorescence (in rfu) versus σ_θ . Horizontal blue line shows the σ_θ values associated to the fluorescence maximum ($\sigma_{\theta\ DCM}$). (f) Relationship between the value of σ_θ at which the DCM occurs ($\sigma_{\theta\ DCM}$, estimated from Figure 2e) and σ_θ at mixed layer when the CHL_{SAT} is maximum ($\sigma^{CHL}_{\theta ML-GODAS}$ estimated from Figure 2b). Color indicates the ratio between $\sigma_{\theta DCM}/\sigma^{CHL}_{\theta ML-GODAS}$.

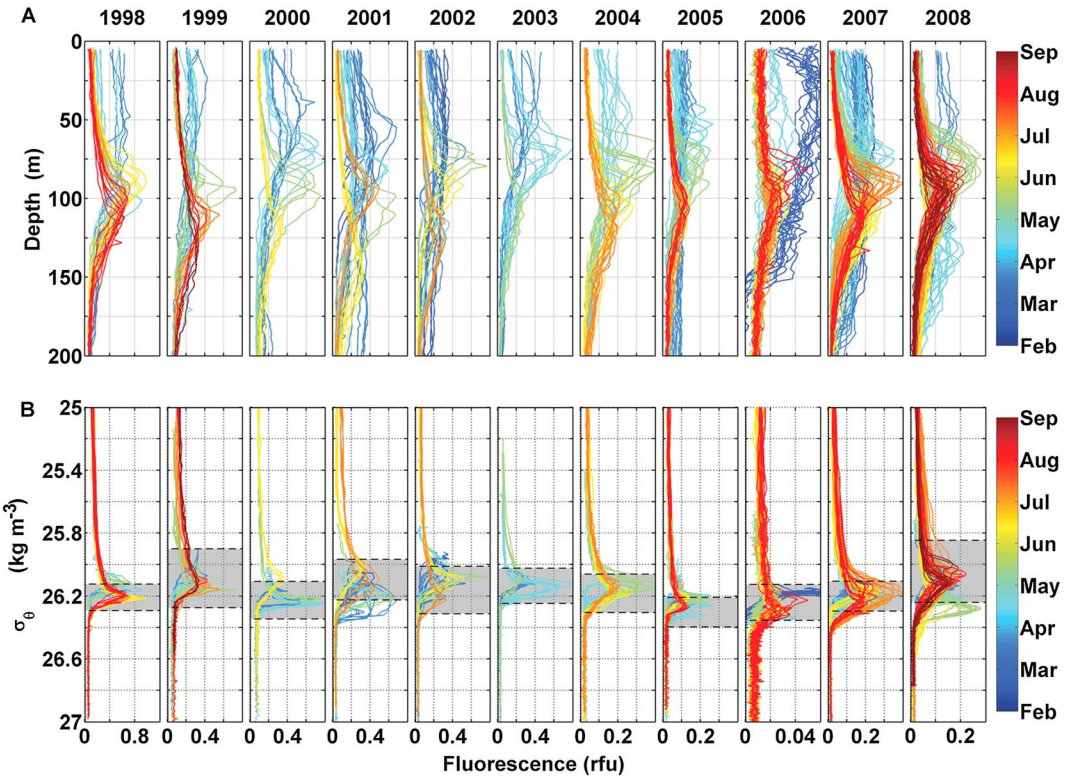

Figure 3. Interannual variability in fluorescence profiles at Station BATS. (a) Fluorescence versus depth and (b) fluorescence versus σ_θ profiles for BATS cruises in the months between the maximum and minimum MLD during a 11 year period (1998–2008). The stippled area in Figure 3b corresponds to the range of σ_θ values in the mixed layer at its maximum depth (normally during February and/or March).

output Global Ocean Data Assimilation System (GODAS) [*Behringer and Xue*, 2004]. The spatial coverage includes a global grid of 418 × 360 horizontal nodes between 65°N and 74°S and 40 levels in depth. The spatial resolution is 0.333 × 1.0° of latitude and longitude, respectively. Density anomaly (σ_θ) is calculated with salinity, potential temperature, and pressure equal to 0, minus 1000 kg m^{-3}. As an example, Figure 2b displays the monthly time series of MLD from GODAS (MLD_{GODAS}) and the average density anomaly ($\sigma_{\theta\ ML-GODAS}$) in the mixed layer for one station located in the North Atlantic (Figure 2a). Supporting information also provides a Google Earth file (File S1) that allows the visualization of this information in each analyzed position (> 9000 open ocean stations).

4. Satellite-Derived Chlorophyll *a*

[9] Weekly surface chlorophyll *a* data were provided from the GlobColour Archive (http://www.globcolour.info/), which produces global ocean color maps (Level-3) by merging data from the three sensors Sea-viewing Wide Field-of-view Sensor, Moderate Resolution Imaging Spectroradiometer, and Medium-Resolution Imaging Spectrometer over the whole globe (4.6 km spatial resolution). Surface chlorophyll *a* data correspond to product chlorophyll *a* case I water based on Garver-Siegel-Maritonera (GSM) merging method [*Maritorena and Siegel*, 2005; *Maritorena et al.*, 2010]. This method provides the best fit to in situ chlorophyll *a* concentration and has the added advantages of providing other products, allowing concomitantly the calculation of pixel-by-pixel error bars. With these data sets, the cloud cover is reduced, and therefore, more useful images become available. Figure 2b shows an example of the annual time series of surface chlorophyll *a* (CHL_{SAT} in mg m^{-3}) at the station located in the North Atlantic.

5. CTD Profiles

[10] Publicly available CTD profiles with fluorescence data from the period comprised between 1998 and 2008 were obtained from several sources (Table 1). Figure 1 displays the position of CTD profiles and Figures 2c–2f shows an example of one of the analysis performed for a station located in the North Atlantic. For each CTD station, the biomass profile (CHL(z), Figure 2d), derived from fluorescence profiles (Figure 2c) after scaling by satellite chlorophyll *a*, were fitted to a shifted Gaussian distribution function ($CHL_{Gaussian}$, Figure 2d) [*Platt et al.*, 1988]:

$$\mathrm{CHL}(z) = B_0 + \frac{h}{\sigma(2\pi)^{1/2}} \exp\left[-\frac{(z-z_m)^2}{2\sigma^2}\right] \quad (1)$$

where B_0 is the background pigment, z_m is the depth of the chlorophyll maximum, σ is a measure of the thickness or vertical spread of the peak, and h is the total pigment within the peak. We defined the depth above and below the DCM as $z_m - 1.5\sigma$ and $z_m + 1.5\sigma$, respectively [*Bouman et al.*, 2000].

[11] In addition, the density anomaly associated with the DCM ($\sigma_{\theta\ DCM}$) was obtained for each CTD cast (Figure 2e). For each profile, this $\sigma_{\theta\ DCM}$ was compared with $\sigma^{CHL}_{\theta\ ML-GODAS}$,

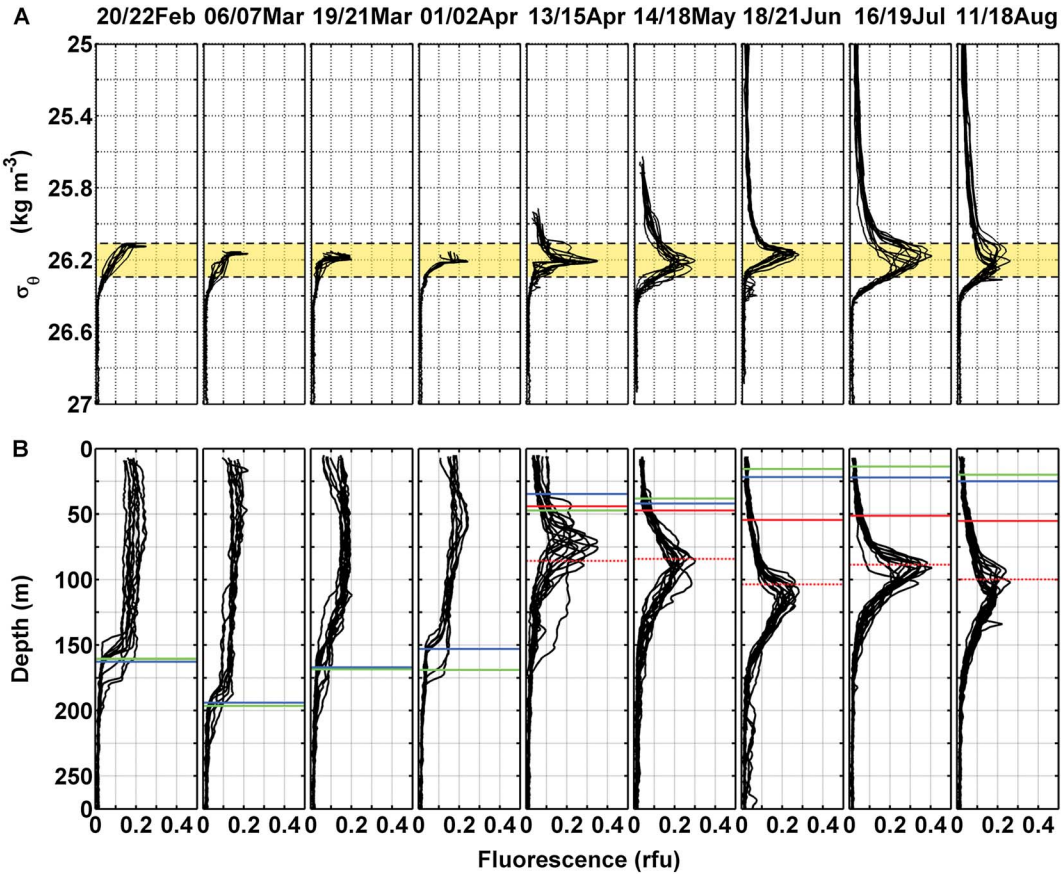

Figure 4. Time course of the biogeochemical variables at Station BATS during 2007. (a) Fluorescence versus σ_θ and (b) fluorescence versus depth profiles for BATS cruises between the maximum and minimum MLD during 2007. Yellow shading indicates the range of σ_θ values in the mixed layer at its maximum depth (February-March). The mean MLD and Brunt-Väisälä maxima are represented by green and blue horizontal lines, respectively. Depths of the 10% and 1% PAR isolumes are represented by solid and dashed red horizontal lines, respectively. No PAR data were available for cruises between February and early April.

which represents the value of $\sigma_{\theta\,\mathrm{ML\text{-}GODAS}}$ at the same location at the time when the surface chlorophyll *a* was at its maximum ($\mathrm{CHL_{max}}$, Figure 2b). Figure 2f shows an example of the ratio $\sigma_{\theta\,\mathrm{DCM}}/\sigma^{\mathrm{CHL}}_{\theta\,\mathrm{ML\text{-}GODAS}}$ at the station located in the North Atlantic.

[12] The mixed layer depth (MLD) for CTD casts obtained from Bermuda Atlantic Time-series Study (BATS) and Hawaii Ocean Time-series (HOTS) databases was calculated by finding the first depth where $\sigma_\theta(D_{\mathrm{mld}}) - \sigma_\theta(0) = \alpha\ \Delta T$; where α is the coefficient of thermal expansion at sea surface conditions and ΔT is chosen to be 0.5°C [*Siegel et al.*, 1995; *Sprintall and Tomczak*, 1992]. CTD casts included in the analysis of the BATS area were those profiles within 30 km of the nominal BATS location [*Michaels and Knap*, 1996; *Steinberg et al.*, 2006]. The Brunt-Väisälä or buoyancy frequency was calculated by

$$N = (g/\rho\ \mathrm{d}\rho/\mathrm{d}z)^{1/2} \tag{2}$$

where g is the acceleration due to gravity, ρ is the density, and z is the depth [*Mann and Lazier*, 1991]. In addition, the depths of the 10% and 1% photosynthetically available radiation (PAR) isolumes were calculated from Bermuda Bio-Optics Project (BBOP) data (Table 1) [*Siegel et al.*, 1995].

[13] The light intensity at each depth (I_z) is described by the Lambert-Beer law [e.g., *Kirk*, 1994].

$$I_z = I_0 \exp[F(z)]. \tag{3}$$

[14] I_0 denotes the light intensity just below the water surface and $F(z)$ is the constant of proportionality [*Lewis et al.*, 1983] based on all components that absorb light, including the water itself and chlorophyll *a*:

$$F(z) = -\left(K_w z + K_c \int_0^z \mathrm{CHL}(z)\mathrm{d}z\right) \tag{4}$$

where K_w (0.03, m^{-1}) and K_c (0.016, $(\mathrm{mg\,chl\,m}^{-3})^{-1}\,\mathrm{m}^{-1}$) are the diffuse attenuation coefficients of pure seawater and the chlorophyll specific attenuation coefficient, respectively [*Bouman et al.*, 2000]. Only casts with an obvious DCM located >1 m deep and an unexplained variance between observed and fitted Gaussian values of $<10\%$ were included in this analysis (4105 profiles from the pool of 9127).

6. Results

[15] Figure 3a shows fluorescence profiles at the Bermuda Atlantic Time-series Study (BATS) between 1998 and 2008

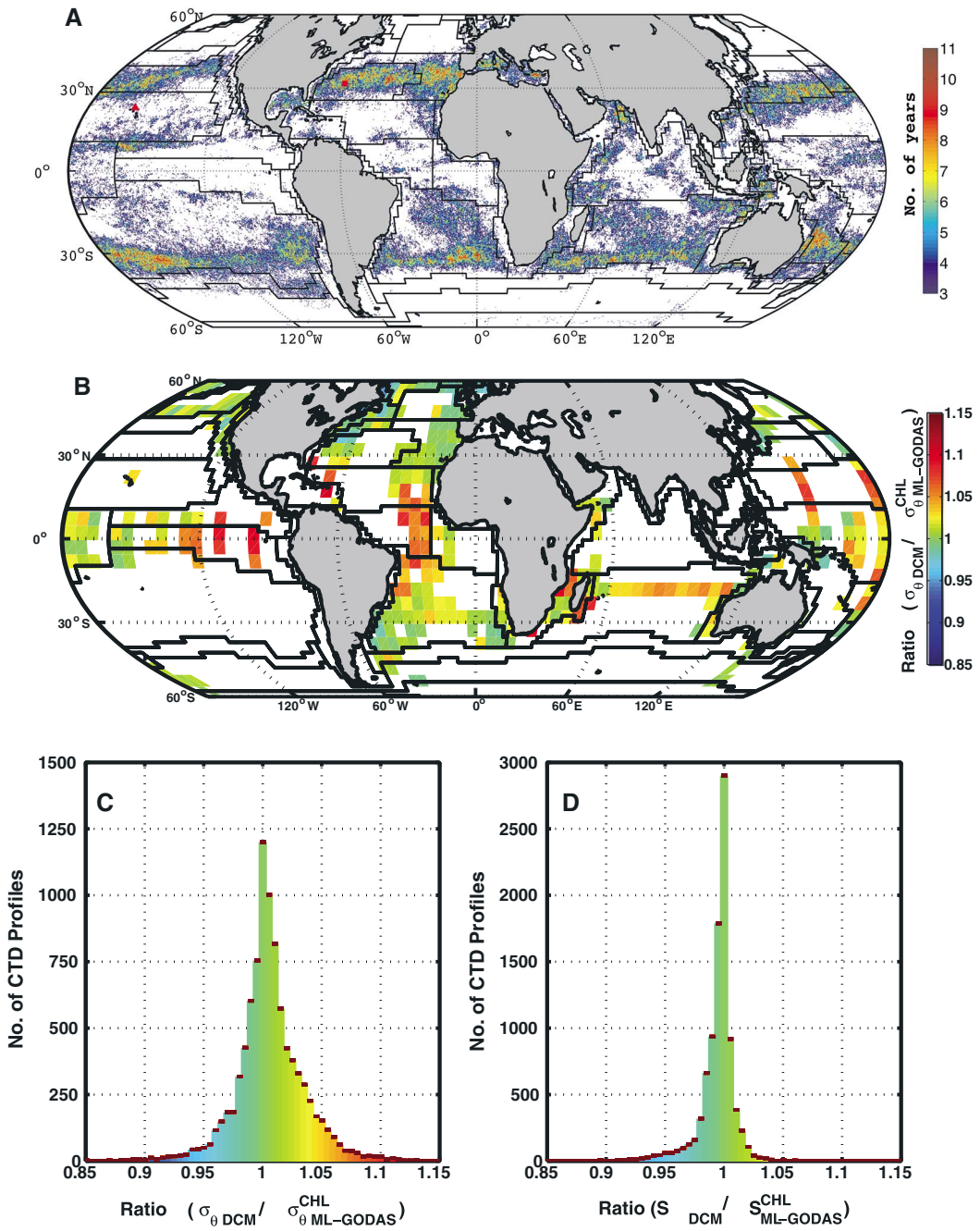

Figure 5. (a) Map of synchronism between MLD_{GODAS} and surface satellite chlorophyll *a* maxima (CHL_{max}). The color scale is the number of years between 1998 and 2008 when both maxima coincide in the same month. Red square and triangle indicates the BATS and HOTS location. (b) Composite map of $\sigma_{\theta DCM}/\sigma^{CHL}_{\theta ML\text{-}GODAS}$ ratios. Background lines in Figures 5a and 5b represent the Longhurst provinces [*Longhurst*, 1998]. (c) Histograms of density anomaly ratios and (d) salinity ratios.

from February/March to August/September, when the mixed layer depth usually reaches its maximum and minimum, respectively. The set of fluorescence profiles is scattered when plotted against pressure, but within each season, chlorophyll maxima converge toward similar σ_θ values (Figure 3b). The particular range of σ_θ where DCMs are found in spring and summer varies for each year; however, it is clearly connected to the density of the previous winter mixed layer (Figure 3b). Some exceptions to this general pattern are also observed but they are connected to exceptional features in water column stratification during the seasonal cycle. Thus, in April of year 2001, there is a second entrainment event after winter whereas the seasonal mixing of 2008 was unusually weak resulting in the presence of a DCM in early March (Figures S1g, S1h, S2i, and S2j, respectively). As an example of the convergence between DCM and the σ_θ values of the mixed layer in the previous winter, Figure 4 shows the fluorescence profiles during 2007 plotted versus σ_θ and depth (Figures 4a and 4b, respectively). The same representation for all years analyzed can be found in Figures S1 and S2. Figure 4 suggests that the

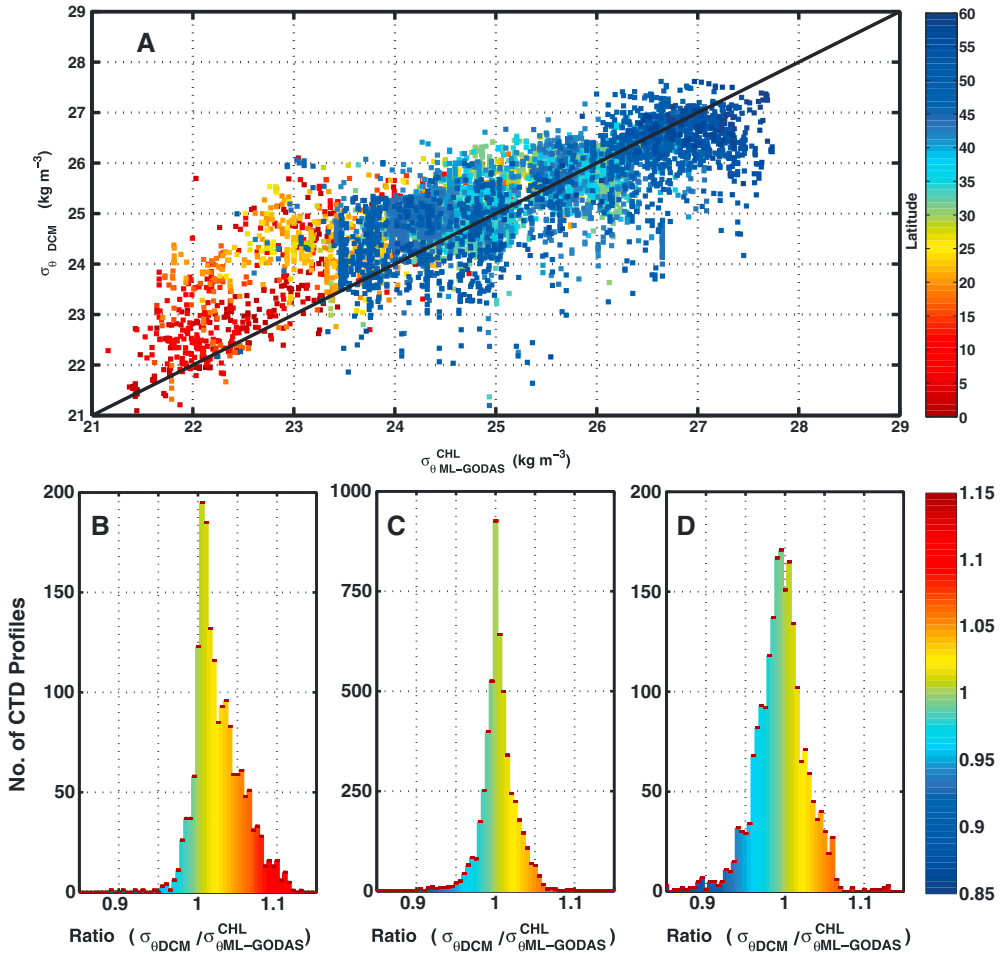

Figure 6. (a) Scatter diagram of $\sigma_{\theta\ \mathrm{DCM}}$ plotted against $\sigma^{\mathrm{CHL}}_{\theta\,\mathrm{ML\text{-}GODAS}}$ for all stations. The line indicates a one-to-one ratio. The color scale indicates the absolute value of the CTD cast latitude. Histograms of latitudinal $\sigma_{\theta\,\mathrm{DCM}}/\sigma^{\mathrm{CHL}}_{\theta\,\mathrm{ML\text{-}GODAS}}$ ratios: (b) between 30°S and 30°N, (c) between 30°N–45°N and 30°S–45°S, (d) between 45°N–60°N and 45°S–60°S.

connection between chlorophyll maxima and surface σ_θ during winter is initiated during this season since high surface-fluorescence (Figure 4b) is recorded during deep mixing in BATS area.

[16] In addition to this area, several sea provinces [in the sense of *Longhurst*, 1998] have annual cycles where the timing of seasonal maxima in MLD and surface chlorophyll *a* concentration coincide. Figure 5a examines this coincidence at global scale through a comparison between the timing of the maximum mixed layer depth ($\mathrm{MLD}^{\mathrm{MAX}}_{\mathrm{GODAS}}$ from GODAS) and peak surface chlorophyll *a* ($\mathrm{CHL}_{\mathrm{max}}$ from GlobColour). The results presented in Figure 5a indicate that these winter blooms are common, particularly in temperate oceans. This suggests that vast regions of the oceans in addition to the BATS area are primed to create spring-summer DCMs at the σ_θ of the previous winter mixed layer.

[17] Although in areas poleward and equatorward of the colored pixels in Figure 5a, there is no coincidence between $\mathrm{MLD}^{\mathrm{MAX}}_{\mathrm{GODAS}}$ and $\mathrm{CHL}_{\mathrm{max}}$, and Figure 5b shows a clear difference between both types of areas. Thus, rather than $\mathrm{MLD}^{\mathrm{MAX}}_{\mathrm{GODAS}}$ and $\mathrm{CHL}_{\mathrm{max}}$, Figures 5b and 5c compare the σ_θ values of the mixed layer when surface chlorophyll is at its maximum ($\sigma^{\mathrm{CHL}}_{\theta\,\mathrm{ML\text{-}GODAS}}$) versus σ_θ at the subsequent DCMs ($\sigma_{\theta\ \mathrm{DCM}}$) derived from the seasonal analysis of more than 9000 CTD profiles (Figure 1). Supporting information provides a Google Earth file (File S1) to allow the visualization of this analysis at each position (an example is provided in Figure 2). The composite map (5° × 5°) of $\sigma_{\theta\,\mathrm{DCM}}/\sigma^{\mathrm{CHL}}_{\theta\,\mathrm{ML\text{-}GODAS}}$ ratio presented in Figure 5b confirms that in the regions where winter blooms occur (Figure 5a), $\sigma_{\theta\ \mathrm{DCM}}$ and $\sigma^{\mathrm{CHL}}_{\theta\,\mathrm{ML\text{-}GODAS}}$ tend to coincide. Figure 5b shows that this coincidence extends poleward of colored regions in Figure 5a but not to regions toward equator.

[18] The histogram of $\sigma_{\theta\,\mathrm{DCM}}/\sigma^{\mathrm{CHL}}_{\theta\,\mathrm{ML\text{-}GODAS}}$ ratio (Figure 5c) demonstrates the high frequency of observations with a ratio very close to one. Analogous histograms are obtained when different water tracers, such as salinity ($S_{\mathrm{DCM}}/S^{\mathrm{CHL}}_{\mathrm{ML\text{-}GODAS}}$), are used (Figure 5d), again reinforcing the similarity of the water characteristics in the mixed layer and subsequent DCMs. However, a scatterplot of $\sigma_{\theta\ \mathrm{DCM}}$ versus $\sigma^{\mathrm{CHL}}_{\theta\,\mathrm{ML\text{-}GODAS}}$ displays latitudinal sensitivity with deviations at waters below 30°, where $\sigma_{\theta\ \mathrm{DCM}}$ is consistently higher than $\sigma^{\mathrm{CHL}}_{\theta\,\mathrm{ML\text{-}GODAS}}$ (Figure 6a). Histograms of the $\sigma_{\theta\,\mathrm{DCM}}/\sigma^{\mathrm{CHL}}_{\theta\,\mathrm{ML\text{-}GODAS}}$ ratio confirm this latitudinal difference between waters below and above 30°; waters toward

the equator of 30° show significant deviations from a ratio of one (Figures 6b–6d, respectively).

7. Discussion

[19] The empirical observations we present provide evidence that DCMs in the temperate ocean cannot be understood without considering how previously described feedbacks for the maintenance of the DCM [*Beckmann and Hense*, 2007, and references therein] will interact with seasonal surface mixing cycle. Our results illustrate the strong link between spring/summer DCMs and previous thermohaline properties of the water in the mixed layer where a bloom has occurred. This link holds both when the bloom occurs during deep mixing (colored pixels in Figure 5a) and when it is associated with the shoaling of the mixed layer after deep mixing (poleward pixels in Figure 5a). This strong connection solidly evidences that the position of DCMs in the temperate ocean cannot be understood without considering the history of formation. None of the mechanisms proposed for the occurrence of DCMs can explain the link reported here if only their instant action, rather than the history of operation, is considered.

[20] For instance, the connection between σ_θ and DCMs with light hypotheses is not sufficient unless the water column history is incorporated [*Bienfang et al*., 1983; *Kirk*, 1983]. There is no evident reason why the σ_θ of a previous mixed layer where a bloom has occurred always happens to have the radiant flux suitable to maintain the DCM, considering the wide vertical range that such σ_θ may occupy in a depth-decaying light-field (Figure 4b). The same argument is also valid for photo acclimation or differential grazing [*Lorenzen*, 1967]. On the other hand, it is not obvious why physiological adaptations or predatory pressures should always happen in a manner that connects DCMs to the σ_θ of a mixed layer where a bloom occurred. Similarly, DCMs are usually associated to nutriclines [*Takahashi and Hori*, 1984] but it is not clear why these nutriclines always occur at that σ_θ [*Navarro et al*., 2006].

[21] Thus, all these features can only be explained by considering hysteresis effects. Hypotheses for DCM occurrence that involve pycnoclines, such as a decrease in settling velocity [*Jerlov*, 1959] or mixing intensity [*Mann and Lazier*, 1991], could explain the constraining of DCMs to a certain σ_θ without invoking their history of formation. However, these are very unlike explanations since DCMs are uncoupled from the observed maxima of Brunt-Väisäla frequency or the mixed layer depth (Figure 4b). The seasonal history of the water column has been suggested to fit the DCMs at the depth of the winter mixed layer [*Kiefer and Kremer*, 1981]. However, a history effect connected to depth cannot explain the constraining of DCMs with certain σ_θ. In particular, it cannot explain why DCMs follow a fixed $\sigma_{\theta\,\mathrm{DCM}}$ in a certain region even though the $\sigma_{\theta\,\mathrm{DCM}}$ dramatically changes depth in that region (Table S2 compiles examples of DCMs constrained at a specific σ_θ for different ocean regions). A history effect based on depth predicts a fixed depth for the DCM while the DCM observation suggests vertical movement forced by ocean dynamics.

[22] Therefore, rather than establishing the spring and summer DCM position at the depth of the winter mixed layer [*Kiefer and Kremer*, 1981], we propose that hysteresis effects link chlorophyll maxima to the σ_θ of the mixed layer where a bloom has occurred. Within ocean regions where seasonal phytoplankton blooms occur during deep mixing (colored pixels in Figure 5a), the link between the nutricline and σ_θ in the winter mixed layer is an immediate consequence of nutrient assimilation just before a stable water column is fully established [*Behrenfeld*, 2010]. Phytoplankton growth and nutrient use during quiescent meteorological windows in late winter, just before stable stratification develops [*Townsend et al*., 1992], creates the interface between waters with low and high nutrients at the density of the winter mixed layer. This interface triggers the connection between DCMs and the value of σ_θ at the winter mixed layer. Similarly, in waters where the Sverdrup model holds [*Sverdrup*, 1953] and the phytoplankton bloom occurs during shoaling of the MLD after deep mixing (pixels poleward of the colored in Figure 5a), the connection is established between DCMs and σ_θ of the mixed layer at the time when the bloom occurs. This chlorophyll *a* maximum maintains the vertical interface between waters with low and high nutrients at the density anomaly of the surface mixed layer.

[23] Once established, DCMs become self-preserving structures [*Beckmann and Hense*, 2007], we propose that this self-preserving capacity is strong enough to fix their position at the σ_θ of initial formation (that of the mixed layer where a bloom has occurred) despite large vertical displacements and changes in the physical environment. Feedback loops that act to stabilize DCMs occur via the attenuation of downwelling irradiance and uptake of upwelling nutrients, producing suboptimal conditions for phytoplankton growth above and below the DCM [*Beckmann and Hense*, 2007]. Indeed, the role of DCMs as nutrient traps in poorly mixed water columns is clear [*Anderson*, 1969; *Anderson et al*., 1969], and detailed numerical simulations have confirmed this [*Jamart et al*., 1977; *Klausmeier and Litchman*, 2001] to such an extent that it is DCMs which are now considered to control the depth of the nutricline rather than the other way around [*Klausmeier and Litchman*, 2001]. Similarly, DCMs are also highly efficient at regulating downwelling irradiance (Figure 7a). At the deepest vertical horizon of DCMs, downwelling irradiance is greatly reduced (Figure 7b).

[24] Therefore, DCMs strongly act to modify their local physical and chemical environment, hampering phytoplankton growth above and below their location, and thus stabilizing their position in the water parcel where they were initially created. In ocean regions where the DCM is not seasonally dissipated by deep mixing (pixels equatorward of the colored in Figure 5a), there is no connection between DCMs and the σ_θ of a previous mixed layer where a bloom has occurred (Figures 6a and 6b). This is the case for the HOTS area, where the mixed layer does not punctuate the DCM during the seasonal cycle (Figure 8) and the DCM are not constrained to a certain σ_θ (Figure S3). This is a common pattern in the North Pacific subtropical gyre, where the depth of the mixed layer rarely penetrates the base of the euphotic zone [*Winn et al*., 1995; *Letelier et al*., 2004].

[25] The rationale above does not exclude the proposed hypotheses for the DCM occurrence (photoaclimation, grazing, motility, pycnocline, settling of phytoplankton, light, nutricline, etc.) but emphasizes the need to understand the consequences of its operation history. The consideration of hysteresis effects offers a simple framework by which the

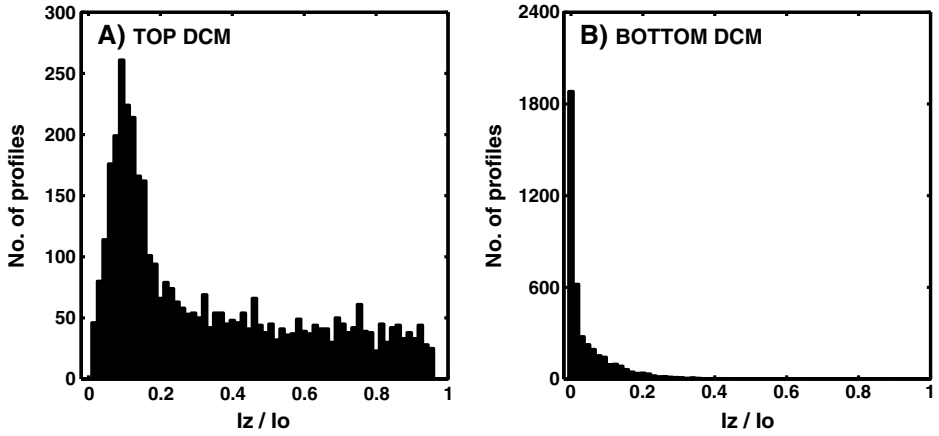

Figure 7. Histogram of the proportion of surface irradiance [I_z/I_o, equation 4] at the (a) top and (b) bottom of the DCM.

connection between DCMs and σ_θ can be understood in the temperate ocean. Furthermore, the proposed hypothesis can also eloquently explain many smaller-scale oceanographic phenomena. For example, dramatic shifts in DCM depth and intensity, which closely follow mesoscale changes in isopycnal depth as observed in the Gulf of Cádiz [*Navarro et al*., 2006] or the CalCOFI area [*Hodges*, 2006]; or changes in DCM depth at the edges of North Atlantic fronts [*Fasham et al*., 1985], where seasonal history of the water masses determines the σ_θ in the mixed layer and thus $\sigma_{\theta\ \mathrm{DCM}}$ on either side of the front. In fact, the $\sigma_{\theta\ \mathrm{DCM}}$ for the Eastern Atlantic Water is higher than the $\sigma_{\theta\ \mathrm{DCM}}$ for Western Atlantic Water, 26.50 and 26.38 kg m^{-3}, respectively [*Fasham et al*., 1985]; the salinity in the eastern part of the front is higher as result of the influence of the saline Mediterranean waters. Hysteresis is also a key component in the explanation of the connection of $\sigma_{\theta\ \mathrm{DCM}}$ between basins. Because of the flow through the Strait of Gibraltar, $\sigma_{\theta\ \mathrm{DCM}}$ values in the central Alborán Sea are different than the western Mediterranean but similar to the Gulf of Cádiz [*Macias et al*., 2008].

[26] The awareness that DCMs are linked by hysteresis to the σ_θ of surface waters also has the potential to improve the diagnosis of ocean biogeochemical cycles. New remote sensing tools like Soil Moisture and Ocean Salinity [*Font et al*., 2010] and Aquarius/Satélite de Aplicaciones Científicas (SAC)-D sensors [*Lagerloef et al*., 2008], which provide global coverage of surface salinity, together with temperature data from operating radiometers, will allow the surface density of temperate seas to be derived, and hence the isopycnal of subsequent DCMs. Consequently, in temperate regions, information about the three-dimensional distribution of biochemical variables can potentially be derived from remote sensing of surface water properties. This advance is highly relevant for climatic projections, where physical simulations have less uncertainty than their biological counterparts [*Lynch et al*., 2009]. By tightly coupling DCMs to the history of physical fields, hysteresis ameliorates our capacity to project the biological impact of future climate scenarios, particularly when these foresee an ocean where winter mixing and stratification will be modified [*Sarmiento et al*., 2004].

[27] In conclusion, our analysis shows that the association between spring/summer DCMs and the σ_θ of a previous mixed layer where a bloom has occurred emerges from the seasonal history of the water column. Hysteresis cannot be ignored and DCM occurrence cannot be understood solely from the instantaneous response of phytoplankton to vertical gradients in physical and chemical fields. Rather than reacting to instantaneous physical forcing, these results indicate that self-preserving of DCMs [*Beckmann and Hense*, 2007] constrains chlorophyll maxima to the σ_θ of the mixed layer

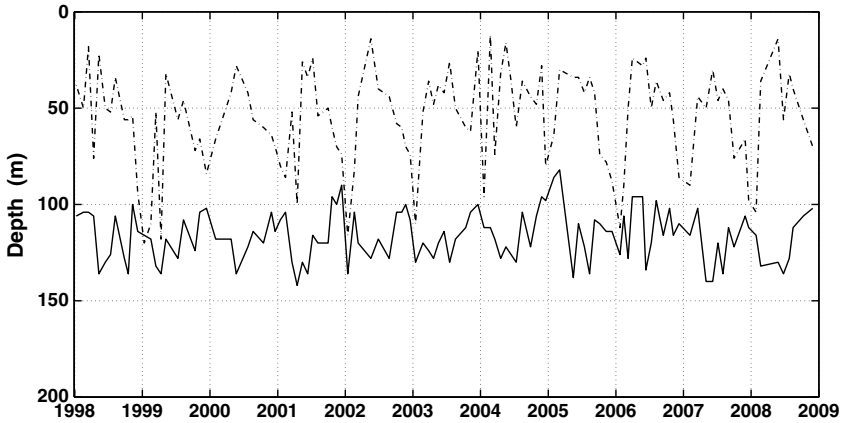

Figure 8. Monthly time series of the depths of MLD (dash-dotted line) and DCM (solid line) for HOTS cruises during a 11 year period (1998–2008).

where a bloom has occurred. This process is strong enough to fix the position of DCMs at that σ_θ despite large vertical displacements imposed by ocean dynamics. Combined with the use of remote sensors to measure salinity and temperature in the surface ocean, this new understanding of the DCM dynamics may improve the quantification of three-dimensional primary production via satellites. This significant enhancement of the representation of oceanic biological processes can also allow increasingly realistic predictions of future biogeochemical scenarios in a warming ocean.

[28] **Acknowledgments.** We are grateful to I.E. Huertas, D. Macias, E.P. Morris, L. Prieto, A. Vázquez for critical review and R. García for help with the supporting information. We also appreciate the comments of the anonymous reviewers that have greatly improved the manuscript. The analysis presented here was supported by research programs including SESAME (FP6-036949), MedEX (CTM2008-04036-E/MAR), PR11-RNM-7722, and CTM2008-05680-C02/MAR. We also thank GODAS, GlobColour, and the databases whose public data made it possible to pose the hypothesis presented here.

References

Anderson, G. C. (1969), Subsurface chlorophyll maximum in the northeast Pacific Ocean, *Limnol. Oceanogr.*, *14*, 386–391.

Anderson, G. C., T. R. Parsons, and K. Stephens (1969), Nitrate distribution in the subarctic Northeast Pacific Ocean, *Deep Sea Res.*, *16*, 329–334.

Beckmann, A., and I. Hense (2007), Beneath the surface: Characteristics of oceanic ecosystems under weak mixing conditions—A theoretical investigation, *Prog. Oceanogr.*, *75*(4), 771–796.

Behrenfeld, M. J. (2010), Abandoning Sverdrup's critical depth hypothesis on phytoplankton blooms, *Ecology*, *91*(4), 997–1021.

Behringer, D., and Y. Xue (2004), Evaluation of the global ocean data assimilation system at NCEP: The Pacific Ocean. *Eighth Symposium on Integrated Observing and Assimilation Systems for Atmosphere*, *Oceans, and Land Surface*, AMS 84th Annual Meeting, Washington State Convention and Trade Center, Seattle, Washington, 11–15.

Bienfang, P., J. Szyper, and E. Laws (1983), Sinking rate and pigment responses to light-limitation of a marine diatom: Implications to dynamics of chlorophyll maximum layers, *Oceanologica acta*, *6*(1), 55–62.

Bouman, H. A., *et al*. (2000), Bio-optical properties of the subtropical North Atlantic. II. Relevance to models of primary production, *Mar. Ecol. Prog. Ser.*, *200*, 19–34.

Cullen, J. J. (1982), The deep chlorophyll maximum: Comparing vertical profiles of chlorophyll *a*, *Can. J. Fish. Aquat. Sci.*, *39*, 791–803.

Fasham, M., T. Platt, B. Irwin, and K. Jones (1985), Factors affecting the spatial pattern of the deep chlorophyll maximum in the region of the Azores front, *Prog. Oceanogr.*, *14*, 129–165.

Font, J., et al. (2010), SMOS: The challenging sea surface salinity measurement from space, *Proc. IEEE*, *98*(5), 649–665.

Hodges, B. A. (2006), On the distribution of oceanic chlorophyll. Ph. D. Dissertation, Univ. of California, San Diego, Calif.

Huisman, J., N. N. Pham Thi, D. K. Karl, and B. Sommeijer (2006), Reduced mixing generates oscillations and chaos in the oceanic deep chlorophyll maximum, *Nature*, *439*, 322–325.

Jamart, B. M., D. F. Winter, K. Banse, G. C. Anderson, and R. K. Lam (1977), Theoretical study of phytoplankton growth and nutrient distribution in the Pacific Ocean off the northwestern U.S. coast, *Deep-Sea Res.*, *24*(8), 753–773.

Jerlov, N. G. (1959), Maxima in the vertical distribution of particles in the sea, *Deep-Sea Res.*, *5*, 173–184.

Kiefer, D. A., and J. N. Kremer (1981), Origins of vertical patterns of phytoplankton and nutrients in the temperate, open ocean: A stratigraphic hypothesis, *Deep Sea Res.*, *28*(10), 1087–1105.

Kirk, J. T. O. (1983), *Light and photosynthesis in aquatic ecosystems*, Cambridge Univ. Press, Cambridge, U. K. and New York.

Kirk, J. T. O. (1994), *Light and photosynthesis in aquatic ecosystems*, 2nd ed., Cambridge Univ. Press, Cambridge, U. K.

Klausmeier, C., and E. Litchman (2001), Algal games: The vertical distribution of phytoplankton in poorly mixed water columns, *Limnol. Oceanogr.*, *46*(8), 1998–2007.

Lagerloef, G., et al. (2008), The Aquarius/SAC-D Mission: Designed to meet the salinity remote-sensing challenge, *Oceanography*, *21*(1), 68–81.

Letelier, R. M., D. M. Karl, M. R. Abbott, and R. R. Bidigare (2004), Light driven seasonal patterns of chlorophyll and nitrate in the lower euphotic zone of the North Pacific Subtropical Gyre, *Limnol. Oceanogr.*, *49*, 508–519.

Lewis, M. R., J. J. Cullen, and T. Platt (1983), Phytoplankton and thermal structure in the upper ocean: Consequences of nonuniformity in chlorophyll profile, *J. Geophys. Res.*, *88*, 2565–2570.

Longhurst, A. R. (1998), *Ecological Geography of the Sea*, Academic Press, San Diego, Calif.

Lonhgurst, A. R., and W. G. Harrinson (1989), The biological pump: Profiles of plankton production and consumption in the upper ocean, *Prog. Oceanogr.*, *22*(1), 47–123.

Lorenzen, C. J. (1967), Vertical distribution of chlorophyll and phaeo-pigments: Baja California, *Deep-Sea Res.*, *14*, 735–745.

Lynch, D., D. J. McGillicuddy Jr., and F. E. Werner (2009), Skill assessment for coupled biological/physical models of marine systems, *J. Mar. Syst.*, *76*(1–2), 1–3.

Macias, D., L. M. Lubian, F. Echevarria, I. E. Huertas, and C. M. Garcia (2008), Chlorophyll maxima and water mass interfaces: Tidally induced dynamics in the Strait of Gibraltar, *Deep Sea Res., Part I*, *55*, 832–846.

Mann, K. H., and J. R. N. Lazier (1991), *Dynamics of Marine Ecosystems*, Blackwell Scientific Publications, Boston, Mass.

Maritorena, S., and D. Siegel (2005), Consistent merging of satellite ocean color data sets using a bio-optical model, *Remote Sens. Environ.*, *94*, 429–440.

Maritorena, S., O. H. F. d'Andon, A. Mangin, and D. A. Siegel (2010), Merged satellite ocean color data products using a bio-optical model: Characteristics, benefits and issues, *Remote Sens. Environ.*, *114*, 1791–1804.

Mellard, J. P., K. Yoshiyama, E. Litchman, and C. A. Klausmeier (2011), The vertical distribution of phytoplankton in stratified water columns, *J. Theor. Biol.*, *269*(1), 16–30.

Michaels, A. F., and A. H. Knap (1996), Overview of the U.S. JGOFS Bermuda Atlantic Time-Series Study and the Hydrostation S program, *Deep Sea Res., Part II*, *43*, 157–198.

Navarro, G., *et al*. (2006), Basin-scale structures governing the position of the deep fluorescence maximum in the Gulf of Cadiz, *Deep Sea Res., Part II*, *53*, 1261–1281.

Platt, T., S. Sathyendranath, C. M. Caverhill, and M. R. Lewis (1988), Ocean primary production and available light: Further algorithms for remote sensing, *Deep Sea Res., Part I*, *35*(6), 855–879.

Riley, G. A., H. M. Stommel, and D. F. Bumpus (1949), Quantitative ecology of the plankton of the western North Atlantic, *Bull. Bingham Oceanogr. Collect.*, *12*(3), 1–169.

Ryabov, A. B., L. Rudolf, and B. Blasius (2010), Vertical distribution and composition of phytoplankton under the influence of an upper mixed layer, *J. Theor. Biol.*, *263*(1), 120–133.

Sarmiento, J. L., et al. (2004), Response of ocean ecosystems to climate warming, *Glob. Biogeochem. Cycle*, *18*, GB3003, doi:10.1029/2003GB002134.

Siegel, D. A., A. F. Michaels, J. C. Sorensen, M. C. O'Brien, and M. A. Hammer (1995), Seasonal variability of light availability and utilization in the Sargasso Sea, *J. Geophys. Res.*, *100*, 8695–8713.

Sprintall, J., and M. Tomczak (1992), Evidence of the barrier layer in the surface layer of the tropics, *J. Geophys. Res.*, *97*, 7305–7316.

Steele, J. H., and C. S. Yentsh (1960), The vertical distribution of chlorophyll, *J. Exp. Mar. Biol. Ecol.*, *39*, 217–226.

Steinberg, D. K., C. A. Carlson, N. R. Bates, R. J. Johnson, A. F. Michaels, and A. H. Knap (2006), Overview of the U.S. JGOFS Bermuda Atlantic Time-series Study (BATS): A decade-scale look at ocean biology and biogeochemistry, *Deep Sea Res., Part II*, *48*, 1405–1447.

Sverdrup, H. U. (1953), On conditions for the vernal blooming of phytoplankton, *ICES J. Mar. Sci.*, *18*, 287–295.

Takahashi, M., and T. Hori (1984), Abundance of picophytoplankton in the subsurface chlorophyll maximum layer in subtropical and tropical waters, *Mar. Biol.*, *79*(2), 177–186.

Townsend, D. W., M. D. Keller, M. E. Sieracki, and S. G. Ackleson (1992), Spring phytoplankton blooms in the absence of vertical water column stratification, *Nature*, *360*, 59–62.

Winn, C. D., L. Campbell, J. R. Christian, R. M. Letelier, D. V. Hebel, J. E. Dore, L. Fujieke, and D. M. Karl (1995), Seasonal variability in the phytoplankton community of the North Pacific Subtropical Gyre, *Glob. Biogeochem. Cycle*, *9*(4), 605–620.

Yoshiyama, K., and H. Nakajima (2002), Catastrophic transition in vertical distributions of phytoplankton: Alternative equilibria in a water column, *J. Theor. Biol.*, *216*(4), 397–408.